Analysis of the electronic crosstalk effect in Terra MODIS long-wave infrared photovoltaic bands using lunar images

Truman Wilson[a], Aisheng Wu[a], Xu Geng[a], Zhipeng Wang[a], and Xiaoxiong Xiong[b]

[a]Science Systems and Applications Inc., 10210 Greenbelt Road, Lanham, MD 20706, USA
[b]Sciences and Exploration Directorate, NASA/GSFC, Greenbelt, MD 20771, USA

ABSTRACT

The Moderate Resolution Imaging Spectroradiometer (MODIS) is one of the key sensors among the suite of remote sensing instruments on board the Earth Observing System Terra and Aqua spacecrafts. For each MODIS spectral band, the sensor degradation has been measured using a set of on-board calibrators. MODIS also uses lunar observations from nearly monthly spacecraft maneuvers, which bring the Moon into view through the space-view port, helping to characterize the scan mirror degradation at a different angles of incidence. Throughout the Terra mission, contamination of the long-wave infrared photovoltaic band (LWIR PV, bands $27-30$) signals has been observed in the form of electronic crosstalk, where signal from each of the detectors among the LWIR PV bands can leak to the other detectors, producing a false signal contribution. This contamination has had a noticeable effect on the MODIS science products since 2010 for band 27, and since 2012 for bands 28 and 29. Images of the Moon have been used effectively for determining the contaminating bands, and have also been used to derive correction coefficients for the crosstalk contamination. In this paper, we introduce an updated technique for characterizing the crosstalk contamination among the LWIR PV bands using data from lunar calibration events. This approach takes into account both the "in-band" and "out-of-band" contribution to the signal contamination for each detector in bands $27-30$, which is not considered in previous works. The crosstalk coefficients can be derived for each lunar calibration event, providing the time dependence of the crosstalk contamination. Application of these coefficients to Earth-view image data results in a significant reduction in image contamination and a correction of the scene radiance for bands $27-30$. Also, this correction shows a significant improvement to certain threshold tests in the MODIS Level-2 Cloud Mask. In this paper, we will detail the methodology used to identify and correct the crosstalk contamination for the LWIR PV bands in Terra MODIS. The derived time-dependent crosstalk coefficients will also be discussed. Finally, the impact of the correction on the downstream data products will be analyzed.

Keywords: MODIS, crosstalk, radiometric improvements, contamination, calibration, striping, thermal emissive bands (TEBs)

1. INTRODUCTION

The EOS Terra spacecraft was launched on December 18, 1999 carrying a suite of Earth-observing instruments.[1] One of the key instruments, the Moderate Resolution Imaging Spectroradiometer (MODIS), uses 36 spectral bands to continuously image the Earth at wavelengths ranging from 0.4 μm to 14.2 μm.[2] The Terra spacecraft is in a low-Earth, Sun-synchronous orbit, with a nominal altitude of 705 km, an orbital period of approximately 98 minutes, and an equatorial crossing time at 10:30 am local time. Every 2 days, the MODIS instrument acquires an image of the entire Earth's surface, with repeating nadir overpass of the same point on the surface every 16 days, at spatial resolutions of 250 m (bands 1 and 2), 500 m (bands $3-7$), and 1 km (bands $8-36$). MODIS is a cross-track, whisk-broom, scanning radiometer, and acquires images using a rotating, double-sided scan mirror, where each scan produces an image swath that is 10 km wide in the track direction at nadir and 2330 km long cross-track, every 1.478 seconds. The MODIS bands are calibrated using one of a number of on-board calibrators (OBC), which include a solar diffuser (SD) with its degradation measured by a solar diffuser stability monitor (SDSM),[3] blackbody target (BB),[4] and spectroradiometric calibration assembly (SRCA).[5] Also, MODIS uses

Further author information: (Send correspondence to T.W.)
T.W.: E-mail: truman.wilson@ssaihq.com, Telephone: 1 301 867 2120

Earth-view targets[6] and the Moon[7] to characterize the scan mirror degradation at a different angle of incidence (AOI) than those of the OBC.

The MODIS instrument has four focal plane assemblies (FPA), which separate the bands by wavelength and detector type. One such FPA, the long-wave infrared (LWIR) FPA for bands $27-36$, has both photovoltaic (PV) and photoconductive (PC) detectors for bands $27-30$ and $31-36$, respectively. The LWIR PV bands, $27-30$, have center wavelengths that range from 6.7 μm to 9.7 μm and are used primarily to measure water vapor distribution, cloud properties, and ozone concentrations. Over the course of the Terra mission, the LWIR PV bands have shown an increase in the noise-equivalent temperature difference (NEdT), sudden gain changes for the detectors, and an increase in the detector-to-detector differences in the scene radiance retrieval,[8] leading to significant striping in the images.[9–12] Also, for bands 27 and 28, coastlines begin to appear in images late in the mission that were not present in earlier images,[9] as seen in Fig. 1. These ghost images show that there has been a significant increase in the signal contamination between 2010 and the present. Also, since bands 29 and 30 have observed coastline features clearly throughout the entire mission, the ghost images are a good indication that part the signal contamination is coming from these bands.

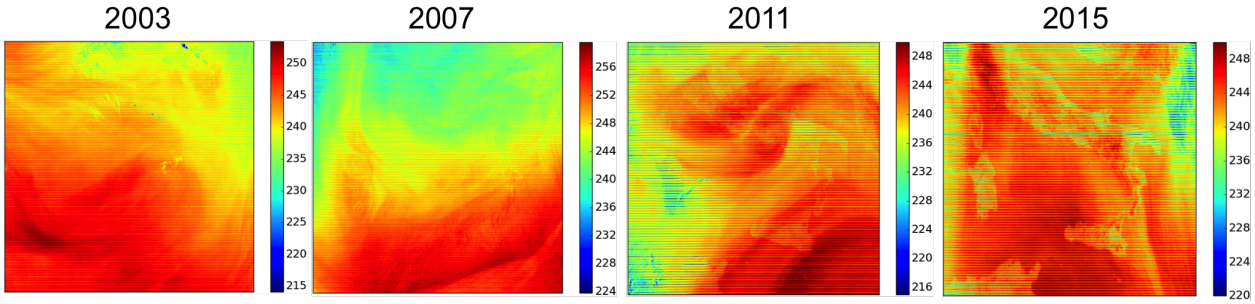

Figure 1. Images for band 27 over the Italian peninsula, the northern coast of Tunisia and the islands of Sicily, Sardinia and Corsica, over the course of the Terra mission. Early in the mission (2003, 2007), there are no land features present in the band 27 images as expected. However, as the magnitude of the crosstalk increases, ghost images of the land features begin to appear more clearly. In the above images, the land features appear faintly in 2011, and then sharply by 2015. Each image was chosen in June/July of their respective years, and was chosen to have minimal cloud cover over the region of interest. The scales to the right of each image show the respective brightness temperature scale in units of Kelvin for each of the images.

The contamination of the LWIR PV bands has been attributed to electronic crosstalk between the bands,[10] as bands $27-30$ share the same sampling electronics on the FPA. Efforts to characterize and correct the signal contamination have been reported previously by Sun, *et. al.* in Refs. 9–12, using observations of the Moon as a means for deriving correction coefficients. These efforts corrected the signal for a given detector in the LWIR PV bands using an "out-of-band" correction that was linearly proportional to the detector-averaged signal from the other LWIR PV bands. These corrections lead to a decrease in the image striping and a significant removal of the ghost image features.

In this paper, we introduce an updated method for characterizing and correcting the crosstalk contamination for all of the LWIR PV bands using lunar images. In this implementation, we account for the contribution to the contamination from detectors within the same band, the need for which is seen in the lunar observation data. The correction of this "in-band" contamination as well as the "out-of-band" contamination leads to an increase in the radiometric bias correction for each LWIR PV band. In particular, the "in-band" correction has a significant impact on band 29, where the contamination within the band is the most significant among all of the LWIR PV bands. The correction algorithm is based on linear correction coefficients using the signal from all four LWIR PV bands as the contamination signal. The correction greatly reduces the image striping from detector-to-detector radiance differences and shows superb removal of the ghost images from bands 27 and 28.

For this paper, we will focus on applying our correction coefficients to scenes in 2015, where the signal contamination is greatest before the Terra safe-mode anomaly, which occurred on February 18, 2016. We will also show the impact of the correction on certain threshold tests in the MODIS Level 2 Cloud Mask.[13] After the

safe-mode anomaly, the contamination increases substantially, particularly for bands 27 and 30. The impact of the safe-mode anomaly and the effectiveness of the correction algorithm after this event are also discussed.

2. DEVELOPMENT OF THE CROSSTALK CORRECTION ALGORITHM

2.1 Characterization of the Crosstalk Effect

Over the course of the Terra mission, there have been near monthly instrument roll maneuvers executed in order to view the Moon through the space-view (SV) port.[7] While these maneuvers are performed so that the response versus scan angle (RVS) for the reflective solar bands (RSB) can be calibrated using the lunar surface reflectance of the Sun, they are also useful for characterizing the LWIR PV crosstalk throughout the mission. The Moon is a bright target against the dark background of space, and is not large enough on the focal plane to illuminate all the LWIR PV bands or detectors simultaneously, as seen in Fig. 2(a). While the actual size of the lunar image on the LWIR focal plane array has some variation throughout the year, it is generally around 6 pixels wide compared to the 10 pixels in the track direction, and the 3 pixels (frames) of separation between each of the bands in the scan direction.

For each band, the lunar image is sampled at different locations on the FPA. As the image is scanned across the FPA, each band will sample the same part of the lunar image at different times, creating a separation in the peak signal for each band with respect to frame number. Also, since the Moon is observed at a much greater distance than the typical Earth-view scene, the lunar image is observed across many scans, whereas the design for Earth-view imaging at nadir is for stitching consecutive scans together to produce a continuous image. On successive scans, the lunar images moves slightly in the track direction, less than the width of a single detector for the 1-km bands.[7] The rate at which the Moon moves in the track direction from scan-to-scan is variable throughout the mission based on the relative velocity and distance of the spacecraft and the Moon. For each detector, the peak observation occurs at different scans/frames. This offset in the peak observation can be used to determine the source of the crosstalk contamination, as anomalous signal appears at scans/frames that should nominally be at the background level.

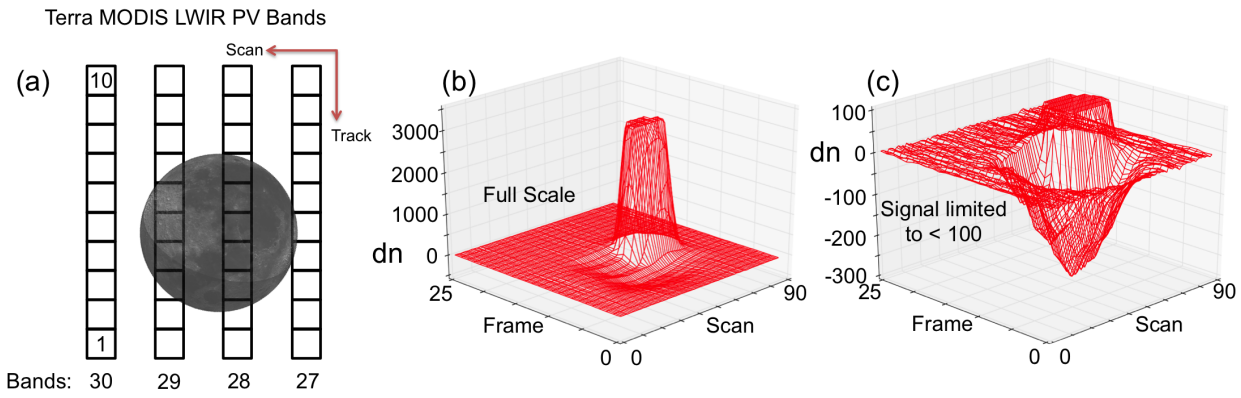

Figure 2. (a) Layout of the LWIR PV bands on the FPA. Each band has 10 detectors aligned in the satellite track direction. The bands are separated along the scan direction, and observe the same scene separated by 3 frames respectively. Superimposed on this figure is an illustration of the Moon,[14] which is scaled to its approximate size on the focal plane, which changes depending on the satellite-Moon distance. In (b)-(c), we show surface plots of the lunar signal as a function of scan number and frame number. This data is taken from the lunar calibration event on August 4, 2015, for band 27, detector 1. In (b), the signal is plotted at full scale and shows digital saturation near the peak. Each band $(27-30)$ shows similar saturation for all detectors, as the scene temperature of the lunar observation is much higher than that of land scenes. In (c), this signal is limited to less than 100 digital counts above the background level in order to show the signal contamination.

For a full lunar observation, we can plot the measured lunar signal for a single detector as a function of scan and frame as seen in Fig. 2(b)-(c). In Fig. 2(b), we can see that measured lunar signal for a given band/detector

is several thousand digital counts above the background level. For the LWIR PV bands, this signal generally saturates and results in a "flat-top" structure near the peak signal. If we focus on the low signal behavior ($<$ 100 counts above background), as seen in Fig. 2(c), we observe that outside of the main lunar signal for this detector, there are many scans/frames where the signal is below the background level. While other forms of signal contamination, such as optical crosstalk,[15] have been observed in other bands in MODIS, this signal comes from electronic crosstalk among the LWIR PV bands, as we will show based on the alignment of the contaminated signal with the signal from the LWIR PV bands.

By determining the scans/frames of the contamination, we can identify which bands/detectors are sending signal to our contaminated detector. Fig. 3(a) shows the contaminated signal for detector 1 of band 27 versus scan and frame, but aligned along the scan direction to show the 3D signal versus frame number. Superimposed on this data are the sending signals from each band at their appropriate frame offsets. In this figure, we can see that the sending bands are all of the LWIR PV bands, bands $27-30$, as we expect. Also, this analysis concludes that there is a significant contribution to the sending signal from the other detectors in the same band as the contaminated detector. This "in-band" sending signal is not considered in previous works,[9–12] and results in a radiometric offset in the corrected signal compared to previous approaches. This effect is present for every detector in bands $27-30$.

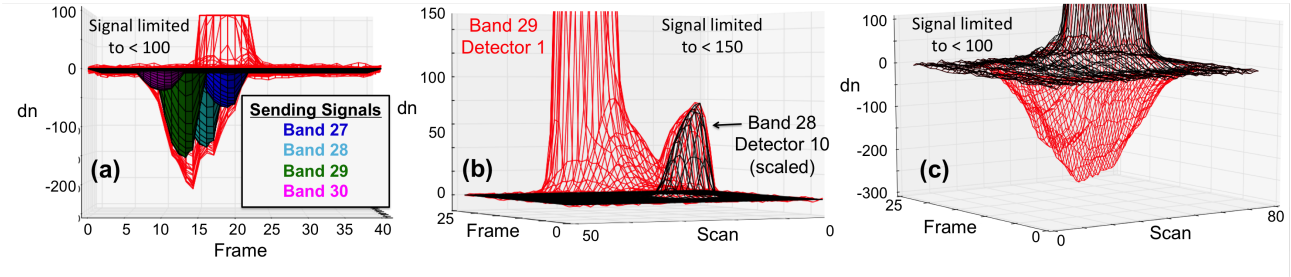

Figure 3. Examples of the contamination signal alignment. In (a), we show the sending signal (bands $27-30$) alignment with the contaminated signal for band 27, detector 1, from August 4, 2015. The sending signals here are scaled to show the alignment with the contaminating signals, and do not reflect the calculated crosstalk coefficients. A saturation correction, using band 31 as a reference, has also been applied to the sending signals. The plot is shown as a 3-dimensional projection along the scan direction in order see both the signal alignment with frame number, and to separate the "in-band" contaminating signal from the main lunar signal on this detector. In (b), we show the anomalous sending signal from band 28, detector 10 to band 29, detector 1 from March 24, 2000. Similar phenomena are also observed for bands 28 and 30. In (c), we show an example of the crosstalk correction applied to the lunar data from (a). The black data is the corrected data and the red data is the uncorrected data.

Our analysis of the sending signal also found an outlying sending signal from bands $27-29$, detector 10 sending to bands $28-30$ detector 1 respectively, throughout the entire mission. An example of this anomalous contaminating signal can be seen in Fig. 3(b) for band 29, detector 1, with the corresponding signal from band 28, detector 10 shown in the same plot. This signal is characteristically different from the other contamination as it is positive relative to the background and nearly constant throughout the entire mission. The precise alignment with the signal from detector 10 of the sending band makes it unlikely that the effect is optical in nature. The effect is likely an electronic sampling error, as the sending and contaminated detectors are sampled in succession with a switching between bands occurring between the sampling. During the switch, the contaminated detector appears to be receiving signal from the sending detector as the electronics are attempting to halt the sampling of the contaminated detector. This effect is not present in band 27, as no switching takes place immediately after the sampling of band 27. This effect is also present in Aqua MODIS, although at a lower magnitude that has a negligible effect on the data.

2.2 Algorithm

After identifying and characterizing the crosstalk contamination signal, the next step is to develop an algorithm for producing correction coefficients that can be applied to restore the Earth-view data. It is important that this

approach is consistent and robust, as we have lunar observations throughout the entire mission that we can use to monitor the changes in the crosstalk contamination. Similar to the approaches taken in previous works,[9–12] the crosstalk contamination signal is assumed to be linearly proportional to the measured signal from the sending detectors. We define the corrected signal from the ith detector as seen in Eq. 1.

$$dn_i(S,F) = dn_i^*(S,F) - \sum_j c_{i,j} \cdot dn_j^*(S, F + \Delta F_j) \tag{1}$$

where dn^* is the measured (contaminated) signal after background subtraction, S and F represent the scan/frame number respectively, j is the sending detector index, $c_{i,j}$ is the crosstalk coefficient matrix, and ΔF_j is the associated frame offset for the sending detector j, which is the same for each detector within a given band. In this formulation, i and j range between $1-40$, representing each detector in bands $27-30$ in product order. The $c_{i,j}$ element for $i=j$ is fixed to zero. While the background signal is also contaminated, this is accounted for in the dn_j^* term in Eq. 1.

To solve for the elements of the $c_{i,j}$ matrix, we compare our contaminated signal to a reference signal, and use the difference to determine the appropriate coefficient values. In this work, we choose our reference signal to be a scaled version of the band 31 signal. Band 31 has no crosstalk contamination and is considered to be a stable reference. We apply scaling factors to this band 31 reference in order to account for differences at low signal between our contaminated bands and band 31 early in the mission, when there is negligible impact due to electronic crosstalk in the LWIR PV bands. With this reference signal, we can solve for $c_{i,j}$ by minimizing the value of χ_i^2 in Eq. 2, for each detector (i).

$$\chi_i^2 = \sum_{S,F} \left(dn_i^*(S,F) - dn_{ref,i}(S,F) - \sum_j c_{i,j} \cdot dn_j^*(S, F + \Delta F_j) \right)^2 \tag{2}$$

Here, the scans/frames that are used in the minimization routine exclude the ones within the main lunar signal. Near the main lunar signal, separating the contaminated signal from the "true" signal becomes difficult, and our comparison to the reference signal becomes less reliable. The scans/frames of the main lunar signal are defined as the scan/frame pairs where the co-registered signal from band 31 is greater than 150 units after background subtraction. Band 31 is used because the signal is typically reduced when the crosstalk contamination increases, which would change the location of the main lunar signal. The initial coefficient matrix is seeded with random values between -0.01 and 0.01, as it was found that seeding with a null matrix lead to a null solution for certain data sets. As of this writing, the solution has been found to converge to a single minimum for all of the available lunar calibration events with the random input solution matrix. The coefficient differences for multiple runs over the same datasets are less than 10^{-7}.

Ideally, this approach would be able to solve for each individual element of the $c_{i,j}$ matrix. However, overlap between the lunar signals in scan and frame between neighboring bands and detectors makes it difficult to separate the contamination coming from each individual detector. For this reason, it was found that fixing the coefficient values for each sending band to the same value produced the most consistent results, particularly for neighboring bands. For non-neighboring bands, a detector-dependent sending signal was explored and found to show little difference as compared to the approach where the coefficient values for each sending detector within a band are fixed to the same value. What difference did arise appeared to be related to an imperfect reference signal, and therefore, we see no advantage in using a detector-dependent approach. For the contamination shown in Fig. 3(b), the coefficients from detector 10 of bands $27-29$ are not fixed with the rest of the coefficients within the band in order to account for the anomalous contamination. The coefficient matrix used in the Level-1B correction code will still maintain values for all detectors sending in case further improvements to the algorithm are made.

After solving for the $c_{i,j}$ matrix, we can test our coefficients by applying them to the lunar data as seen in Fig. 3(c), for band 27, detector 1. The red and black data represent the uncorrected and corrected data respectively. After applying our correction, the negative signal that is seen after background subtraction due to

the contamination is removed completely. For each detector in bands $27 - 30$, the application of the crosstalk coefficients to the lunar data shows similar successful results.

2.3 Trending and Application of the Correction Coefficients

The crosstalk correction coefficients were derived using scheduled observations of the Moon through the SV port on a near monthly basis throughout the entire mission. These coefficients are derived for each receiving detector in the LWIR PV bands independently as described in the previous section. In Fig. 4, an example of the crosstalk coefficients for a selected receiving detector in each of the LWIR PV bands is shown.

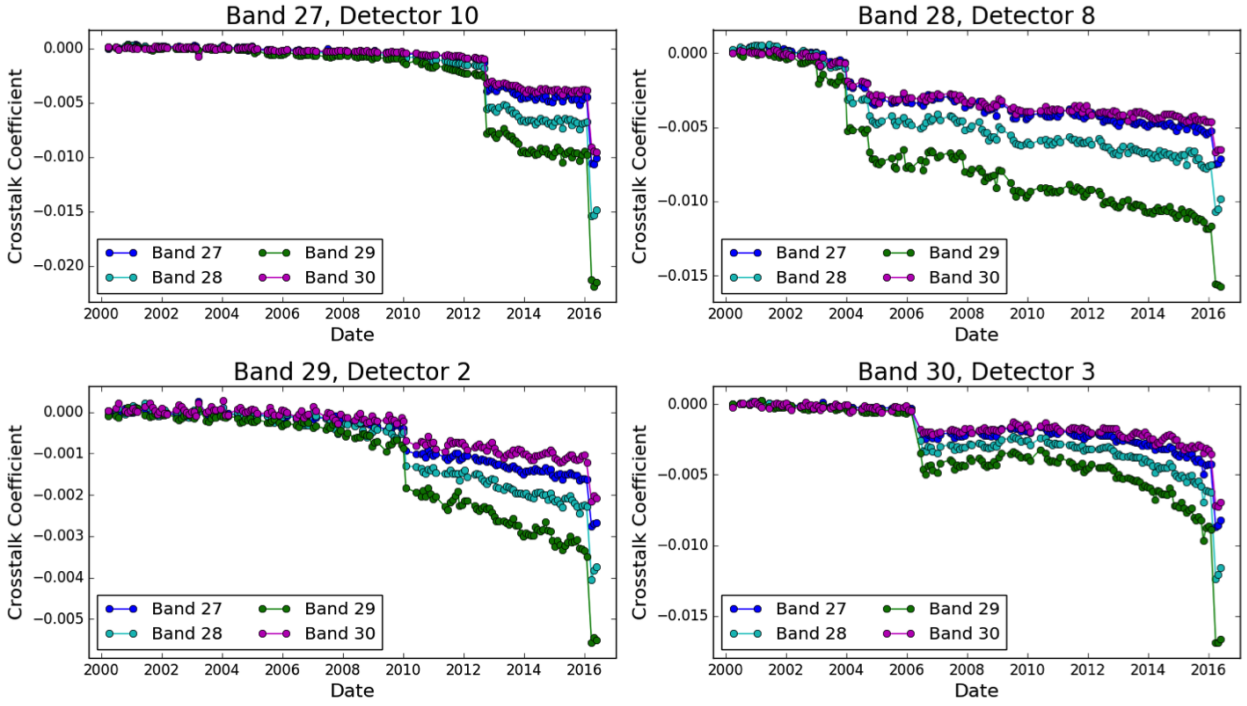

Figure 4. Example trending crosstalk coefficients for a selected receiving detector from each band ($27 - 30$). Each receiving detector has a sending component from each of the 4 LWIR PV bands. The coefficients in the above plots are the result of fixing the coefficient from each sending detector within the band to the same value. For many of the detectors, sudden changes in the crosstalk coefficients occur throughout the mission. In general, these changes occur at different times for each contaminated detector. However, the last sudden change for all detectors is associated with the Terra MODIS safe-mode event on February 18, 2016.

Early in the mission, the impact of electronic crosstalk is relatively small, and the coefficient values are near zero for all detectors. As the mission continues, the crosstalk impact manifests itself through both slow and sudden changes in the coefficient values. These sudden changes occur at different times for each of the detectors in the LWIR PV bands. However, for a given detector, the sudden change in the coefficient values is seen for all of the sending bands simultaneously. Careful examination of the sudden changes in the coefficients have shown that they are related to passage of the spacecraft through the South Atlantic Anomaly (SAA), where the Earth's magnetic field is relatively weakened. This weakened magnetic field leads to a higher flux of high-energy charged particles that can cause damage to spacecraft electronics in low-Earth orbit.

Another property of the crosstalk contamination that can be seen in Fig. 4 is the relative magnitude of the derived coefficients between each of the sending bands for all of the detectors. In general, the absolute values of the crosstalk coefficients are largest for sending band 29, followed by bands 28, 27, and 30, for every detector in the LWIR PV bands. Given this fact, the inclusion of the "in-band" correction for the detectors in band 29 will

have a large impact on the final correction. The cause of this property of the coefficients is currently unknown, and will be the subject of further study.

Since the crosstalk contamination occurs at the raw signal level, any data product or parameter that is derived from the raw data needs to have the crosstalk coefficients applied to correct the data. To provide the proper correction, we must first apply our crosstalk coefficients to the OBC data to re-derive the gain coefficients for the sensors, and then to the retrieved scene data for each granule so that we can compute the scene radiance for the Level 1B data product (L1B). The L1B Earth-view (EV) scene radiance is computed from Eq. 3.[4]

$$L_{EV} = \frac{1}{\mathrm{RVS}_{EV}} \left(a_0 + b_1 dn_{EV} + a_2 dn_{EV}^2 - (\mathrm{RVS}_{SV} - \mathrm{RVS}_{EV})\, L_{SM} \right) \tag{3}$$

where a_0, b_1, and a_2 are the gain coefficients, dn_{EV} is the background subtracted, measured digital signal, RVS is the response versus scan angle for the scan mirror (EV and SV represent the Earth-view and space-view respectively), and L_{SM} is the radiance of the scan mirror, which is calculated using the Planck equation for a measured scan-mirror temperature. The gain coefficients a_0 and a_2 are determined during regularly scheduled (quarterly) BB warm-up/cool-down cycles, which capture the non-linear response of the detector as a function of BB temperature.[4] The gain coefficient b_1 is computed on a scan-by-scan basis using the BB source at a fixed temperature.[4] Each of the gain coefficients, a_0, b_1, and a_2 must be derived from crosstalk corrected data before computing the scene radiance.

The crosstalk correction has a significant impact on the gain parameters for the LWIR PV bands as seen in Fig. 5. For most detectors in the thermal emissive bands, the change in gain on-orbit is relatively small.[4] However, for the LWIR PV bands, each detector sees a change in gain that is closely related to the change in the derived crosstalk coefficients from the lunar events. After applying the crosstalk correction, the gain drift for each of the detectors is greatly reduced, as seen in Fig. 5 for the linear gain term, b_1. Also, the detector-to-detector gain differences are reduced, which helps reduce the image striping after conversion of our measured signal to radiance. The most affected gain parameter is the linear term, b_1. However, the non-linear terms a_0 and a_2 are affected as well, particularly for band 27, detectors 1, 2, 9, and 10, and band 30 detector 8, with the largest change coming after the safe-mode anomaly.

3. IMPACT OF ELECTRONIC CROSSTALK ON L1 AND L2 DATA PRODUCTS

3.1 Image Striping and Artifacts in MODIS L1B

The electronic crosstalk among the LWIR PV bands has a significant impact on the Level 1B calibrated radiance, which has a cascading impact on the higher-level data products derived from this radiance. This contamination has lead to a variety of artifacts in the calibrated images that have changed throughout the lifetime of the mission as the magnitude of the crosstalk has increased. The most general feature of the contamination is increased image striping owing to the receiving detector differences in the magnitude of the contamination. This effect can be seen in for each of the LWIR PV bands. Another contamination feature, the false presence of coastlines in the images, appears in bands 27 and 28.

In this paper, we use the scene brightness temperature, T_b, as the unit for comparison. The brightness temperature is defined as the temperature required of an ideal blackbody source to produce the same measured radiance at a given wavelength, λ. The brightness temperature can be computed from the Earth-view scene radiance from Eq. 4.

$$T_b = \frac{hc}{k_B \lambda} \ln^{-1} \left(1 + \frac{2hc^2}{L_{EV} \lambda^5} \right) \tag{4}$$

where h, c, and k_B are Planck's constant, the speed of light and Boltzmann's constant respectively. The wavelength, λ, is taken to be the center wavelength of the observing band. For bands $27 - 30$, the center wavelengths are 6.72, 7.33, 8.55, and 9.73 μm respectively. For many downstream data products (ex: Cloud Mask[13]), the brightness temperature difference between chosen bands is used as a way to determine scene properties, and thus is a quantity of interest in terms of the offset that is introduced from the crosstalk correction.

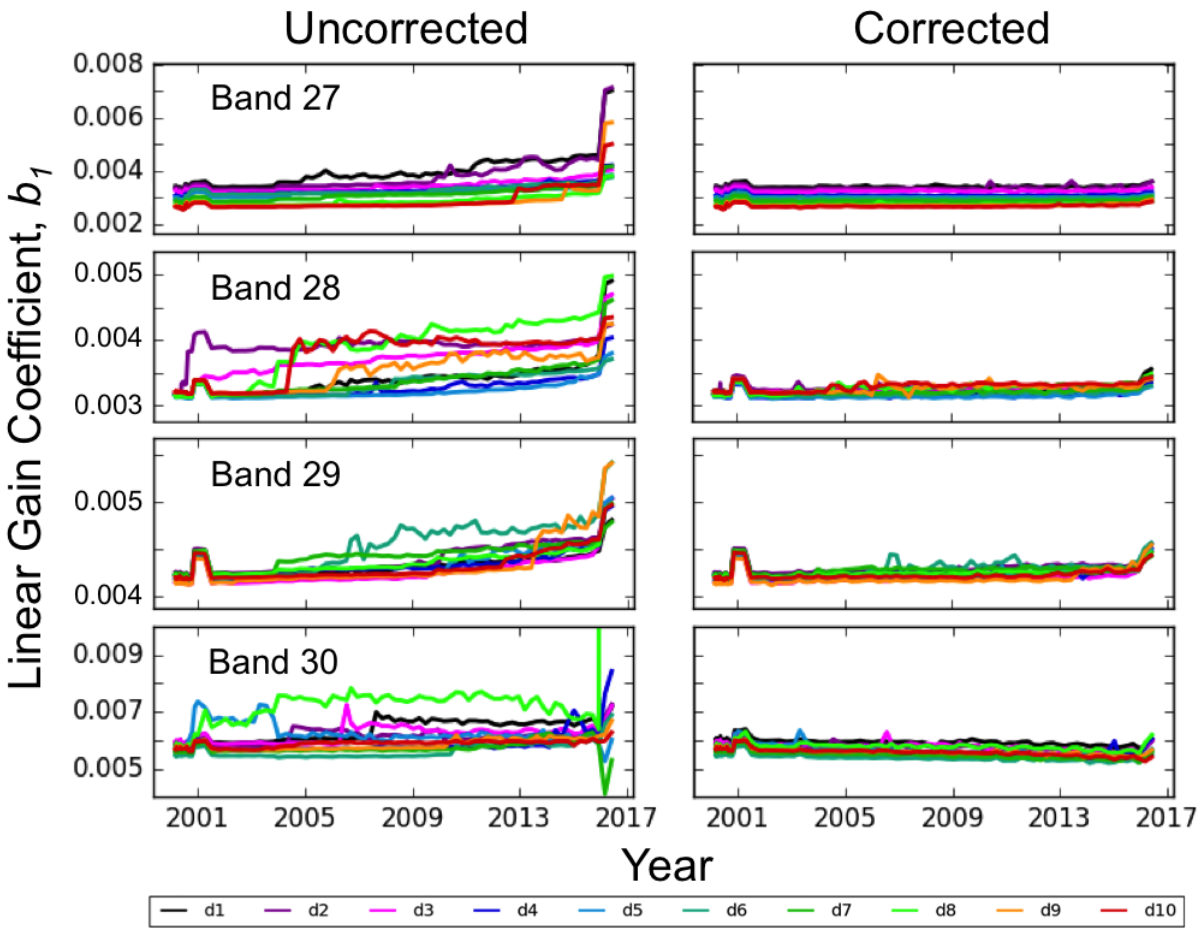

Figure 5. The gain correction for the linear gain parameter, b_1, for bands $27 - 30$. The gain is derived from BB warm-up/cool-down events throughout the mission with corrections for the non-linear gain parameters for a_0 and a_2 applied. For band 30, detector 8, the uncorrected b_1 increases substantially to a value near 0.2. The scale is limited to see the effect of the correction on all of the detectors.

For band 27, there is a high impact on the retrieved images owing to detector-to-detector differences in the contaminating signal. Also, since band 27 is a channel used primarily to measure water vapor in the atmosphere, early in the Terra mission, distinct land features were not observed in the images. However, as the crosstalk contamination increased, these land features began to appear in the data as seen in Fig. 1, from contamination from bands 29 and 30. In Fig. 1, four images over the Italian peninsula in 2003, 2007, 2011, and 2015 are shown. In 2011, we begin to see faint features from the land appear in the image. By 2015, the land features are outlined clearly across the entire image. The presence of these land features late in the mission is a clear indication that electronic crosstalk is the main cause of contamination in the LWIR PV bands.

In Fig. 6(27a), we apply the correction coefficients derived from the lunar data for a granule on July 2, 2015 over the Italian peninsula. After correction, there is a significant reduction in the image striping and also a near complete removal of the false land features, although some faint features still persist in the image. The difference between the uncorrected and corrected images (Fig. 6(27a), right) shows that the land features were a major contributor to the image contamination. A closer examination of the effect of the applied correction is shown in Fig. 6(27b)-(27c) as line profiles of the brightness temperature over vertical (27b) and horizontal pixels (27c). We chose these line profiles over the island of Sardinia, allowing us to determine the extent of the land feature removal. In Fig. 6(27b), the correction reduces detector-to-detector differences in the brightness temperature as

well as introducing radiometric bias in the retrieved brightness temperature of the scene. In Fig. 6(27c), the correction removes nearly all of the land feature ghost image.

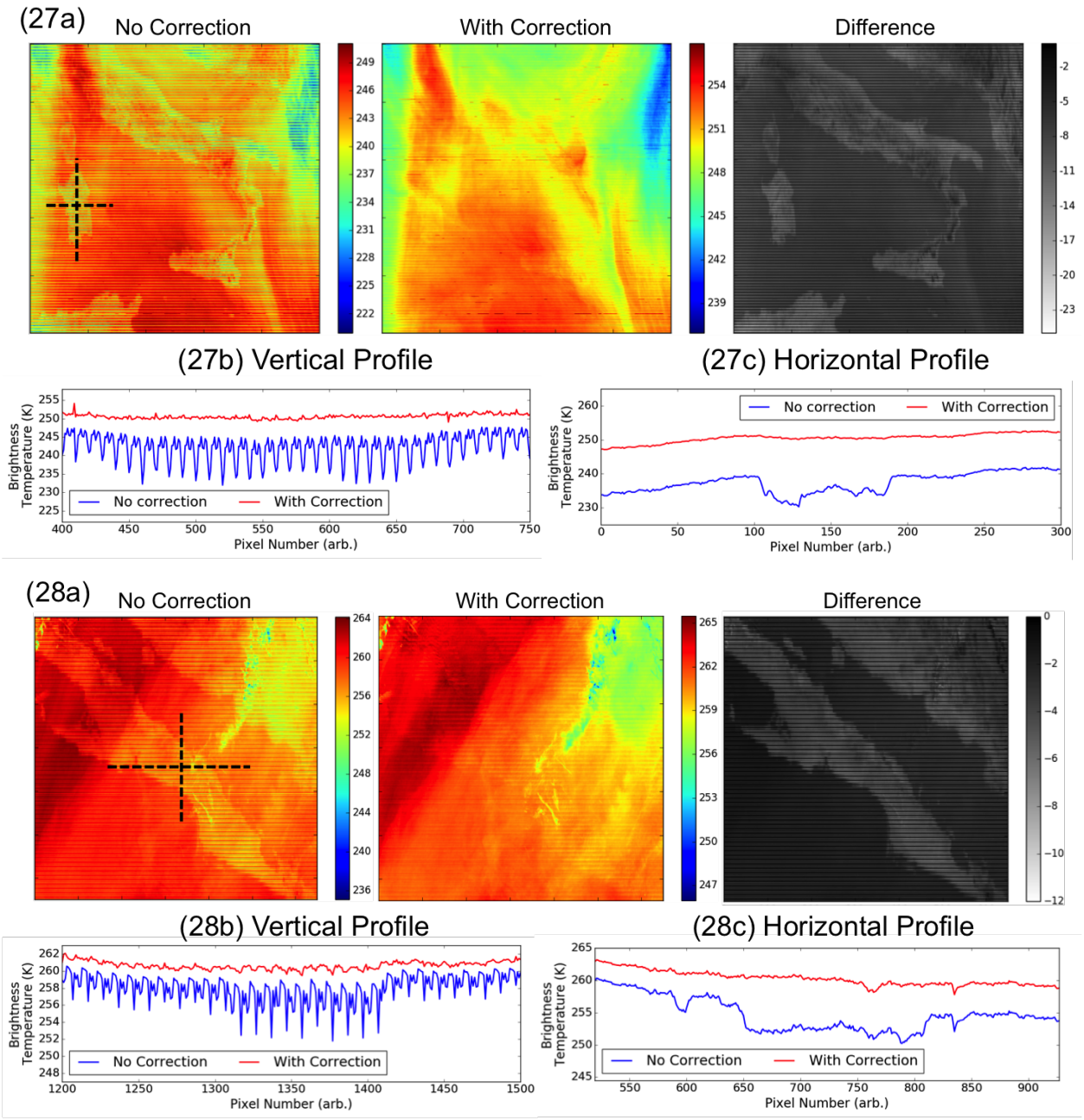

Figure 6. Example image correction for bands 27 and 28, taken over the Italian peninsula (7/2/2015) and Baja peninsula (7/11/2015) respectively. In (a), we show the uncorrected (left) and corrected (center) images with their respective brightness temperature scales in units of Kelvin to the right of each image. The difference image (right) shows the extent of the land feature removal and the overall brightness temperature correction. In (b)-(c), we take horizontal and vertical line profiles over the island of Sardinia (band 27) and the Baja peninsula (band 28), to show the effect of the correction algorithm. The horizontal stripes seen in the images can be seen more clearly in the vertical profiles.

For band 28, the crosstalk contamination is similar to that of band 27, where detector-to-detector differences, radiometric bias, and sharp land features that were not present early in the mission can be seen in the images. The overall effect of the correction is also similar to that of band 27, where the correction reduces the image striping and introduces a positive radiometric bias as seen in Fig. 6. Also, we achieve a significant removal of the sharp land features as seen in Fig. 6(28a), where the corrections were applied to a granule over the Baja peninsula from July 7, 2015.

For bands 29 and 30, the main feature of the crosstalk contamination is image striping owing to detector-to-detector contamination differences as seen in Fig. 7. Again, the crosstalk correction is able to remove most of the detector-to-detector differences, as seen in the line profiles at the bottom of Fig. 7. For band 29, the radiometric correction lowers brightness temperature. For band 30, scene brightness temperatures are typically lower than that of the blackbody OBC, and applying a correction on b_1 and the scene without correcting a_0 and a_2 actually results in greater image striping.[12] For this work, a_0, b_1, and a_2 are corrected for every band and detector.

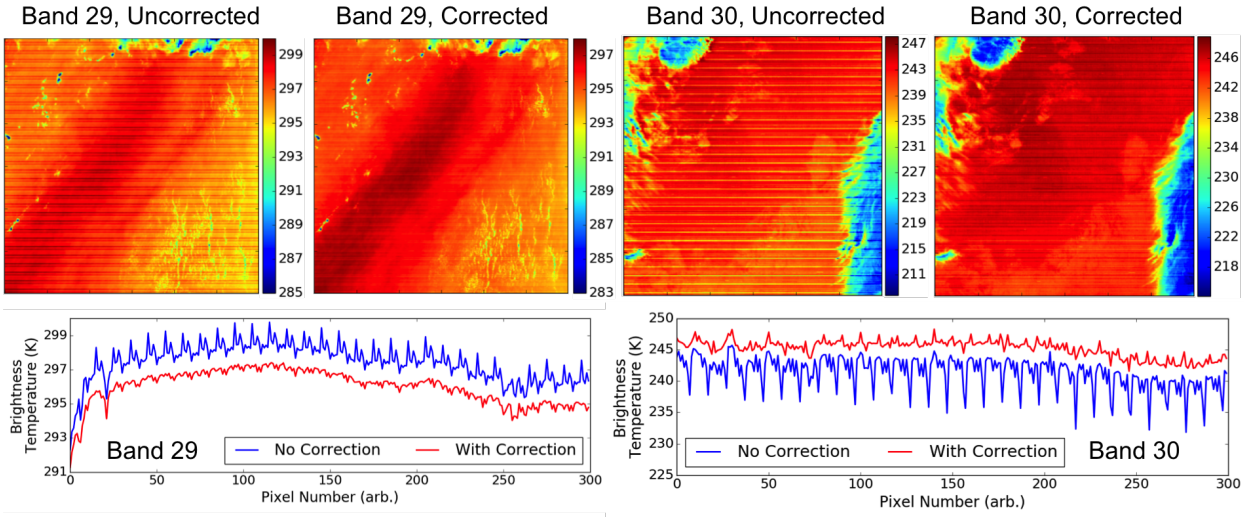

Figure 7. Example image correction for bands 29 and 30 over the Pacific Ocean on July 1, 2015. For band 29 (left), the correction is applied over warm waters, and reduces the detector-to-detector differences. For band 29, the radiometric shift in brightness temperature is towards lower temperatures, unlike the other bands. For band 30 (right), the correction is applied over cold waters near the Antarctica, and also reduces detector-to-detector differences. The lower plots show vertical line profiles through the center of the images for comparison.

For bands 27 and 29, there has also been a consistent drift in the measured brightness temperature over the course of the mission, which is shown for selected granules over the Atlantic ocean in Fig. 8. The granules selected are from warm ocean scenes, where the average brightness temperature of band 31 is greater than 270 K. The drift is measured by taking the difference in brightness temperature with band 31, and normalizing to the data from the year 2000. The drift in bands 27 and 29 are in opposite directions, with the effect being much larger in band 27. The application of the correction coefficients reduces the drift in both bands significantly, which shows that the derived coefficients provide a consistent correction throughout the mission. These radiometric corrections can lead to a significant impact on downstream products derived from MODIS Level-1B as described in the next section.

3.2 Impact on MODIS Level-2 Cloud Mask

The MODIS cloud mask (MOD35_L2 for Terra MODIS) is a Level-2 data product derived from the MODIS Level-1B calibrated radiance, and is used to determine the probability of clear sky on a pixel level.[13] The cloud mask uses radiance data from bands $1-9$, 17, 18, $20-22$, $26-29$, $31-33$, and 35 to perform a variety of tests to determine the presence of many types of clouds. The inclusion of bands $27-29$ in the cloud mask for certain tests means that the crosstalk correction should impact the results of these tests. For some tests, the

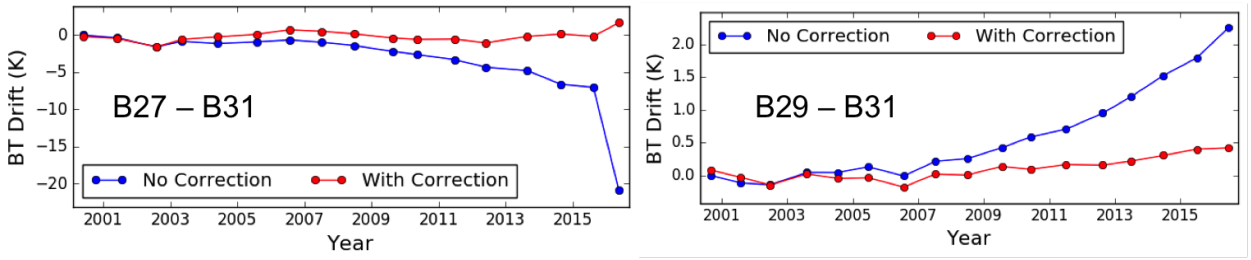

Figure 8. Brightness temperature drift relative to band 31 for bands 27 (left) and 29 (right) for warm Atlantic ocean scenes. For each year of the mission, a single granule is selected that had a brightness temperature difference with band 31 that was near the annual average. The relative brightness temperature difference is normalized to the data from the year 2000.

difference in brightness temperature between two bands measuring at different wavelengths can be sensitive to the presence of clouds, where the cloud can introduce different levels of radiation absorption between the bands.

For this work, we apply the crosstalk correction to derive corrected radiances for the MODIS Level-1B. We then take the corrected radiance data, and perform the tests from the MODIS Level-2 cloud mask described in Ref. 13 in order to assess the impact of the correction. It is important to note that in the official MODIS cloud mask product, some of the highly affected detectors are flagged as noisy or inoperable in order to prevent them from having a large impact on the output of the product. In our analysis, we treat every detector as being in an operable state in order to assess the total impact of the correction.

One test that has shown a significant impact from crosstalk contamination is the 8.6 μm - 11 μm test, which uses the brightness temperature difference between bands 29 and 31 to detect the presence of cirrus clouds.[13] This test is only performed over liquid water surfaces, as variability in the emittance over land surfaces at 8.6 μm lowers the confidence of the cloud mask output. For the B29−B31 cloud mask, brightness temperature differences of less than −1.0 K result in a high confidence of clear sky, and brightness temperature differences greater than 0 K result in a high confidence of the presence of a cloud. In between these two thresholds, the confidence for clear sky/cloud varies linearly, with brightness temperature differences greater than the midpoint of −0.5 K being registered as a cloud. These temperature thresholds have resulted in a high sensitivity to the band 29 brightness temperature on the B29−B31 cloud mask, as the band 29 brightness temperature over warm ocean scenes compared to band 31 has drifted by more than 2 K over the course of the mission, as seen in Fig. 8. Higher brightness temperature as a result of the crosstalk contamination in band 29 results in a higher rate of false cloud detection.

Fig. 9 (top row) shows an example of the B29−B31 cloud mask test in 2015 for a warm ocean scene. The left image in the figure shows a grayscale image of band 31 to show a reference of the total cloud cover. The uncorrected cloud mask, in the center image, shows that nearly the entire image shows a positive cloud detection. Other parts of the image that show striping in the confidence levels are a result of the detector-to-detector differences that arise due to the crosstalk contamination. The corrected cloud mask, in the right image, shows a substantial reduction in the false cloud detection that was seen in the uncorrected data. The corrected data also shows a significant reduction in the striping of the confidence levels. In this case, the corrected cloud mask closely resembles the band 31 image that is seen on the left.

Another cloud mask test that is affected by crosstalk contamination is the 6.7 μm brightness temperature threshold test, which uses the brightness temperature of band 27 to detect thick, high-altitude clouds. This test is performed over all scenes. The thresholds for this cloud mask test for high confidence of clear sky and cloud detection are below 215 K and above 225 K respectively. Again, the confidence level varies between these two levels linearly with a midpoint at 220 K. Although the radiometric bias induced by the crosstalk is relatively large for band 27, since the brightness temperature thresholds are so low for this cloud mask test, for many granules, there is only a very small effect resulting from the crosstalk before the safe-mode anomaly. However, there are still some granules where the effect of the contamination is clear.

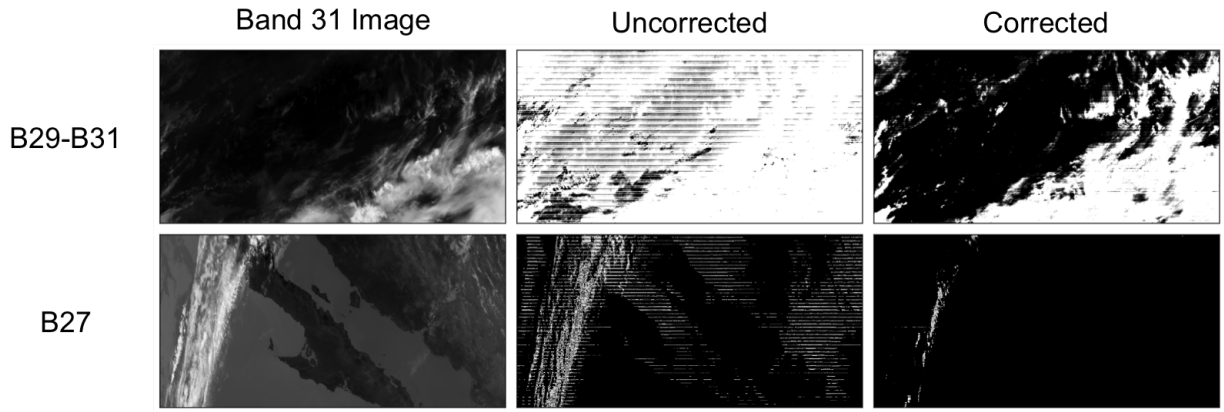

Figure 9. Example of two threshold tests used in the Level 2 cloud mask product. The left image is a grayscale image of band 31 that can be used as a reference of potential cloud cover. Since each test detects different types of clouds, it is not necessarily expected that individual tests will have a cloud mask that closely matches the band 31 image. The center and right images are the result of the cloud mask test on the uncorrected and corrected data respectively. Each test shows pixels ranging from black to white, with black corresponding to high confidence of clear sky and white showing high confidence of clouds. (top) B29−B31 brightness temperature test for the detection of ice clouds over ocean. (bottom) B27 brightness temperature test to detect thick, high-altitude clouds in all scenes.

In in the bottom row of Fig. 9, we show images of the B27 cloud mask test for a granule over the Baja peninsula in 2015. Similar to the contamination effects in the images shown in Fig. 6, the land features should not be present for band 27. However, signal contamination for bands 29 and 30 lower the brightness temperature retrieved from band 27 over these land features. For this cloud mask test, the land features further contaminate the cloud mask test as seen in the center image of Fig. 9. Although the confidence level varies, the outline of the coast of the Baja peninsula and Mexico can be seen clearly in the cloud mask. After correction, all of the land features are removed from the cloud mask data, leaving only the detection of high altitude clouds from the clouds seen in the band 31 image.

Other cloud masks tests, such as the B28−B31 and B28−B29 cloud mask test show little impact from the crosstalk correction for the granules that were tested. These tests involve larger differences in the brightness temperature between the bands, and are less sensitive to the small drifts in the individual bands. Overall, the crosstalk correction provides a significant improvement in the cloud mask tests using bands 27 and 29.

3.3 Impact of the Terra Safe-Mode Anomaly

On February 18, 2016, the Terra spacecraft entered "safe-mode" when an inclination angle maneuver triggered an alarm aboard the spacecraft. During this time, the MODIS nadir door was closed, and the instrument temperature and LWIR focal plane array were allowed to return to ambient temperature. The instrument was successfully transitioned back to science mode on February 24, 2016.

After the return to science mode, the impact of the safe-mode event on the LWIR PV crosstalk contamination was assessed using data from the lunar observation on March 28, 2016. The crosstalk coefficients were derived using the same algorithm, and it was found that the change in the contamination after safe-mode was significant. An example of the crosstalk coefficients is seen in Fig. 4. The large data jump in the derived coefficients seen in early 2016 is due to the safe-mode anomaly, where the magnitude of the coefficients increased by more than a factor of 2 for some detectors. The safe-mode event affected all detectors in bands $27 - 30$.

The safe-mode anomaly had particularly large impacts on band 27, detectors 1, 2, 9, and 10 and band 30, detector 8. For these detectors, the contamination can be large enough to produce signal levels that are lower than the background level, resulting in radiance levels that are not physical. Further analysis shows that these negative signals can result in undefined pixels for images that can be up to 12% of the total number of pixels in the image. After correction, more than 99% of the undefined pixels are restored.

In Fig. 10, images from bands 27 and 30 after the safe-mode with and without the correction applied are shown. Before the correction, the image striping is extreme, with detector-to-detector brightness temperature differences for positive radiance pixels as high as 100 K. Many of the detectors are flagged in the MODIS Level-1B as out-of-family, however, the crosstalk correction appears to reduce the difference between these detectors and the detectors from the rest of the band. The difference between the images before and after the correction is extreme, and the line profiles seen in the bottom of Fig. 10 show that the image striping is greatly reduced. Although some residual image striping remains after the correction is applied for band 27, with brightness temperature differences between detectors on the order of a few Kelvin, the improvement in the image quality is apparent.

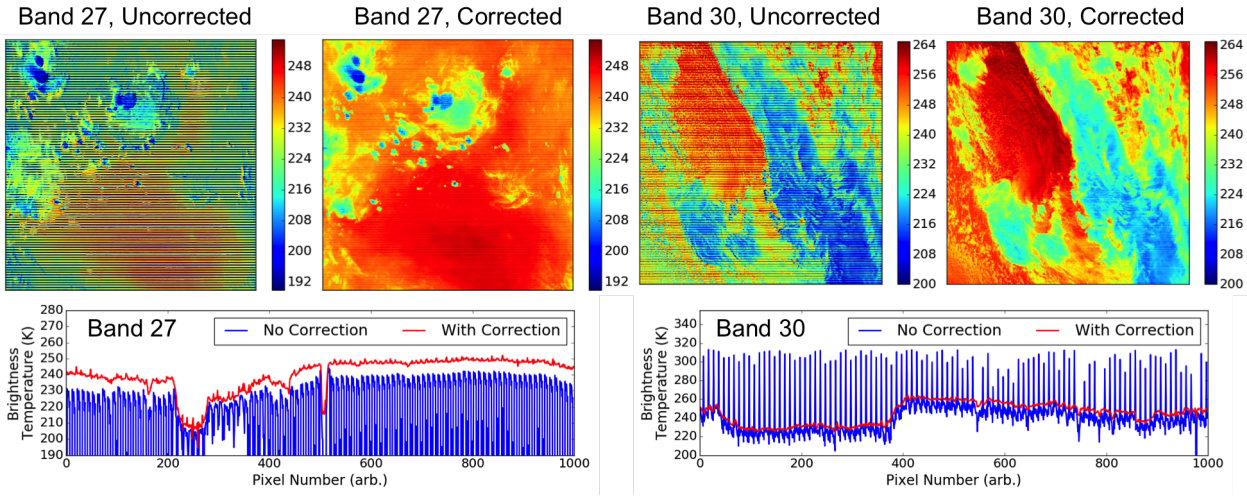

Figure 10. Example image corrections (top) for band 27 and band 30 after the safe-mode anomaly on February 18, 2016. For band 27, the image is from June 17, 2016 over the Pacific Ocean near Indonesia. For band 30, the image is from June 21, 2016, over the South Pacific Ocean. The color scales for the images are fixed to the scale of the corrected image, as undefined pixels, set to a brightness temperature of 0, reduce the contrast of the uncorrected image. The lower plots show vertical line profiles through the center of the images for comparison. The brightness temperature axis of the lower plots is also fixed to a false minimum, as many of the pixels have very low or undefined brightness temperature due to negative radiance retrieval.

For band 30, detector 8 is the main source of the image striping after the safe-mode anomaly. For the granule shown in Fig. 10, the brightness temperature of detector 8 is much higher than the rest of the detectors in the band. Unlike band 27, the direction of the brightness temperature shift is not consistent, and is scene dependent, where some scenes show a shift from detector 8 to much lower brightness temperatures. The downward shift in brightness temperature for detector 8 is typically observed for warm scenes, with brightness temperatures for band 30 above 280 K. This occurs because the crosstalk contamination for band 30 has a greater effect on the offset and non-linear gain terms, a_0 and a_2. The crosstalk correction greatly reduces the detector-to-detector differences among all of the detectors in band 30 and is also able to bring detector 8 back into family with the rest of the band.

For bands 28 and 29, the safe-mode anomaly increased the magnitude of the crosstalk contamination which led to increased detector-to-detector brightness temperature differences and an overall increase in the radiometric bias as compared to before the safe-mode anomaly. However, the effect in these two bands is not as extreme compared to bands 27 and 30.

An increase in the crosstalk contamination due to the safe-mode anomaly also has corresponding impacts on the Level 2 data products. In the case of the Level 2 cloud mask product, the retrieval of false clouds in the band 27 high altitude cloud mask and the B29 − B31 brightness temperature difference test for cirrus clouds increases after the safe-mode anomaly, as seen in Fig. 11. For warm ocean scenes in the B29−B31 test, the increase in the radiometric bias introduced by the crosstalk contamination leads to the detection of clouds over nearly the

entire scene. The correction is able to reduce the false cloud retrieval significantly, and the result after correction is similar to what was obtained before the safe-mode anomaly. For the B27 test, the extreme contamination in detectors 1, 2, 9, and 10 introduces a high level of striping to the cloud mask result before the correction is applied. After correction, the image shows a reasonable level of detection of high-altitude clouds compared to the band 31 image.

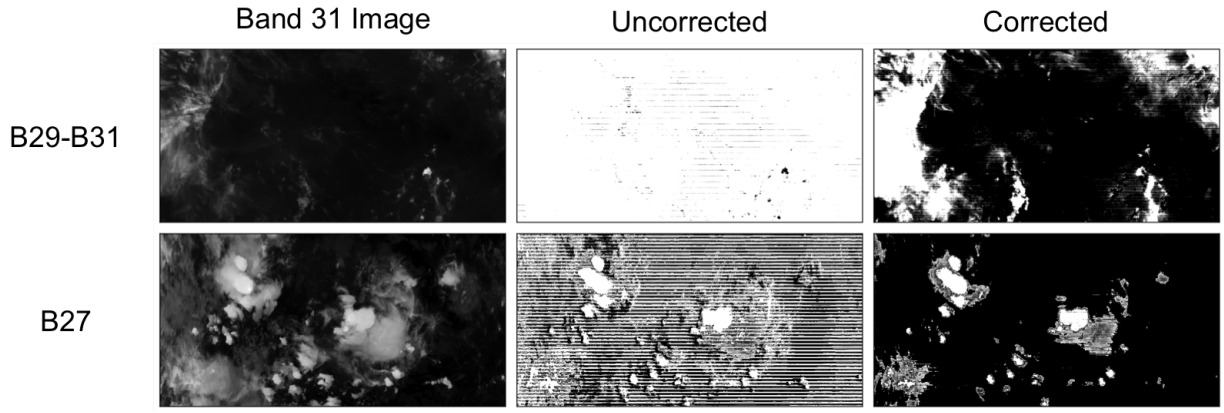

Figure 11. Cloud mask tests after the safe-mode anomaly. The top row shows the B29−B31 cloud mask test. The bottom row shows the B27 cloud mask test. In each case, the increased contamination from the safe-mode anomaly resulted in a much higher rate of false cloud detection. Both scenes are excerpts from the granule 2016169.1340. The thresholds for each test are the same as in the previous example in Fig. 9.

4. SUMMARY

The contamination from electronic crosstalk among the LWIR PV bands has been characterized using lunar observations throughout the Terra MODIS mission. These observations showed that the contaminating signal originated among bands $27-30$, including contamination from other detectors within the same band. The contamination has been increasing for each band and detector throughout the mission, with the safe-mode anomaly on February 18, 2016 resulting in the largest increase in the crosstalk contamination for most of the detectors. The lunar observations have also been used to derive correction coefficients for each detector in bands $27-30$. The crosstalk coefficients were used to re-derive the detector gain coefficients and to apply corrections to the retrieved Earth-view data. These corrections greatly reduced the detector-to-detector differences in the scene radiance as well as corrected the radiometric bias that was a result of the contamination throughout the mission. The correction was also able to remove falsely detected land features from bands 27 and 28 that began to appear late in the mission. We also assessed the impact on the MODIS cloud mask product, showing that the correction greatly reduces the number of false clouds detected, particularly in the B29−B31 test for cirrus clouds. The results of the correction are encouraging, and our goal is to implement the crosstalk correction for the full mission reprocessed in Terra MODIS Collection 7.

ACKNOWLEDGMENTS

The authors would like to thank Chris Moeller of the University of Wisconsin for his support, comments, and suggestions for this work, Na Chen of SSAI for her support in processing the MODIS Level-1B data, and Graziela Keller of SSAI for her comments on this work.

REFERENCES

[1] Barnes, W. L., Xiong, X., and Salomonson, V. V., "Status of Terra MODIS and Aqua MODIS," *Proc. IGARSS* **2**, 970–972 (2002).

[2] Salomonson, V. V., Barnes, W. L., Xiong, X., Kempler, S., and Masuoka, E., "An overview of Earth Observing System MODIS instrument and associated data systems performance," *Proc. IGARSS* **2**, 1174–1176 (2002).

[3] Xiong, X., Sun, J., Barnes, W. L., Salomonson, V. V., Esposito, J., Erives, H., and Guenther, B., "Multiyear on-orbit calibration and performance of Terra MODIS reflective solar bands," *IEEE Trans. Geosci. Remote Sens.* **45**(4), 879 (2002).

[4] Xiong, X., Wu, A., Wenny, B. N., Madhavan, S., Wang, Z., Li, Y., Chen, N., Barnes, W. L., and Salomonson, V. V., "Terra and Aqua MODIS thermal emissive bands on-orbit calibration and performance," *IEEE Trans. Geosci. Remote Sens.* **53**(10), 5709 (2015).

[5] Link, D., Wang, Z., and Xiong, X., "Status of MODIS spatial and spectral characterization and performance," *Proc. SPIE* **9881**, 98811G–1 (2016).

[6] Chen, H., Xiong, X., Angal, A., Geng, X., and Wu, A., "Alternative method of on-orbit response-versus-scan-angle characterization for MODIS reflective solar bands," *J. Appl. Remote Sens.* **10**(2), 024004 (2016).

[7] Sun, J., Xiong, X., Barnes, W., and Guenther, B., "MODIS reflective solar bands on-orbit lunar calibration," *IEEE Trans. Geosci. Remote Sens.* **45**(7), 2383 (2007).

[8] Xiong, X., Chiang, K., Wu, A., Barnes, W. L., Guenther, B., and Salomonson, V. V., "Multiyear on-orbit calibration and performance of Terra MODIS thermal emissive bands," *IEEE Trans. Geosci. Remote Sens.* **46**(6), 1790 (2008).

[9] Sun, J., Madhavan, S., Wenny, B. N., and Xiong, X., "Terra MODIS band 27 electronic crosstalk: Cause, impact, and mitigation," *Proc. SPIE* **8176**, 81760Z (2011).

[10] Sun, J., Madhavan, S., Xiong, X., and Wang, M., "Electronic crosstalk correction for terra long wave infrared photovoltaic bands," *Proc. SPIE* **9264**, 926412 (2014).

[11] Sun, J., Madhavan, S., Xiong, X., and Wang, M., "Investigation of the electronic crosstalk in Terra MODIS band 28," *IEEE Trans. Geosci. Remote Sens.* **53**(10), 5722 (2015).

[12] Sun, J., Madhavan, S., and Wang, M., "Investigation and mitigation of the crosstalk effect in Terra MODIS band 30," *Remote Sens.* **8**(3), 249 (2016).

[13] Ackerman, S., Frey, R., Strabala, K., Liu, Y., Gumley, L., Baum, B., and Menzel, P., "Discriminating clear sky from cloud with MODIS, algorithm theoretical basis document (MOD 35, Collection 6)." http://modis-atmos.gsfc.nasa.gov/_docs/MOD35_ATBD_Collection6.pdf (October 2010).

[14] Robinson, M. et al., "Lunar reconnaissance orbiter camera (LROC) instrument overview," *Space Sci. Rev.* **150**, 81–124 (2010).

[15] Li, W., Xiong, X., Chiang, K., and Toller, G., "Evaluation of Terra MODIS PC bands optical leak correction algorithm," *Proc. SPIE* **5882**, 191–199 (2005).